applied optics

Multi-plane, multi-band image projection via broadband diffractive optics

MONJURUL MEEM,[1,†] APRATIM MAJUMDER,[2,†] AND RAJESH MENON[2,*]

[1]Department of Electrical and Computer Engineering, University of Utah, Salt Lake City, Utah 84112, USA
[2]Oblate Optics, Inc., San Diego, California 92130, USA
*Corresponding author: rmenon@eng.utah.edu

Received 23 August 2019; revised 29 October 2019; accepted 15 November 2019; posted 18 November 2019 (Doc. ID 376076); published 23 December 2019

We demonstrate visible and near-IR image projection via non-absorbing, multi-level broadband diffractive-optical elements (BDOEs) in one or more planes. By appropriate design of the BDOE topography, we experimentally demonstrate (1) different images in different spectral bands, (2) different images in different image planes, (3) image magnification by changing the distance between the illumination source and the BDOE, (4) completely flat BDOE via an index-contrast top coating, and (5) reflective BDOEs. All of these are accomplished with broadband illumination. Furthermore, the BDOEs are highly efficient and versatile and can be inexpensively mass manufactured using imprint-based replication techniques.

https://doi.org/10.1364/AO.59.000038

1. INTRODUCTION

Broadband image projection can be achieved with absorbing color filters as in conventional image projectors. However, these are very inefficient. The same may be achieved with non-absorbing patterned dielectrics, which can be programmable (e.g., spatial-light modulators) [1] or fixed (generally referred to as holograms or computer-generated holograms). Traditionally, these devices are sensitive to the wavelength of illumination, achieving high efficiencies only in narrow bandwidths (requiring lasers for their effective operation). Recently, there have been several attempts to improve the broadband performance of such devices either by using metamaterials [2,3] or via multi-level diffractive structures [4,5]. Metamaterials-based holograms require deep subwavelength minimum features and relatively large aspect ratios, which render them very challenging for practical applications and are also very inefficient, [6] especially when the mechanism is based on plasmonics.

We previously demonstrated the design, fabrication, and characterization of multi-level diffractive devices that can project full-color images when illuminated by collimated white light [4,5]. The constituent element of such a broadband diffractive-optical element (BDOE) is typically a square pixel, whose minimum width is determined by the fabrication technology and whose height is determined via a nonlinear optimization procedure. The nonlinear optimization is based on the modified direct-binary-search algorithm that we have described previously in detail [4,5]. The goal of optimization is to maximize the diffraction efficiency averaged over all the wavelengths of interest. In order to ensure manufacturability, we enforce additional constraints on the number of height levels. By exploiting the intrinsic chromaticity of diffraction as well as material dispersion, here we show that it is possible to achieve efficient image projection with temporally incoherent and spatially partially coherent illumination. The specific advancements that are reported here are the projection of a full-color image by illumination with the white-LED flashlight of a mobile phone, of two distinct images in the visible and in the invisible (near-infrared) bands, and of multiple distinct images in multiple planes. Intriguingly, we show the equivalence of our BDOE with a lens whose point-spread function (PSF) is structured as an image. This equivalence enables magnification of the projected images without any additional optics. We further showcase the versatility of BDOEs by demonstrating a completely flat device based on an index-contrast top coating and also a reflective BDOE. All the devices reported here have minimum feature width of 20 μm (except one in Fig. 5, which has 10 μm), maximum feature height of 2.6 μm, and 100 levels. All other parameters are listed in Table S1 in Ref. [7]. However, it is important to note that BDOEs can be designed for any feature size as small as $\lambda/2$ (beyond which, all free-space modes are evanescent). In contrast to diffraction gratings and far-field diffractive elements (including conventional holograms), our BDOEs are designed in the Fresnel regime. Therefore, the conventional diffraction efficiency (which is typically defined as a function of spatial frequency) is not meaningful. Instead, here we use the imaging efficiency (see Ref. [7] for details), which is a measure of the fidelity of the projected image and is computed in

real space [4]. In addition, we also report the measured transmission/reflection efficiency as a function of wavelength (>96%) and confirm that our BDOEs also function as anti-reflection coatings for certain wavelengths.

2. EXPERIMENTAL RESULTS FOR FULL-COLOR, MULTI-BAND, AND MULTI-PLANE IMAGE PROJECTION

Each BDOE is comprised of square pixels whose heights are determined by a nonlinear optimization method to maximize imaging efficiency [4]. The BDOEs are fabricated in a transparent photopolymer film (positive-tone photoresist S1813 from Microchem with a maximum thickness of 2.6 μm) placed atop a 50.8-mm-diameter soda-lime glass wafer (thickness ~0.5 mm). Direct laser write grayscale-optical lithography was used for patterning the BDOEs [4]. For characterization, the BDOEs were illuminated with an appropriate source and the projected images were recorded. For further details about the fabrication and experimental characterization of the BDOEs, please refer to Ref. [7].

Figure 1 shows a BDOE that is designed to project a saturated-color image when illuminated by the white-LED flashlight of a mobile phone. The image was projected onto a white screen and photographed and then compared to the simulated image. Rich saturated colors spanning the entire visible range (blue, green, red) are clearly visible. As others have reported previously, [8] one can increase spatial coherence to improve image quality. Increasing the source–BDOE distance can increase the spatial coherence. In Fig. 1, we placed the phone (emission area diameter about 3 mm) about 0.9 m away from the BDOE to obtain collimated white light. At lower spatial coherence (closer source–BDOE distances), the same image is formed but with reduced sharpness as expected [8]. This device was also tested under direct sunlight, and the same colorful image is observed (see Fig. S8 in Ref. [7]). The pixel heights for all the devices were measured using a stylus profilometer, and these measurements confirm that the standard deviation of the pixel-height error is less than 65 nm (data included in Section 3 in Ref. [7]). Our experiments confirm that one can use the flashlight of any mobile phone to project colorful images, which have not been demonstrated by meta-holograms or conventional holograms. We also note that all our devices are on axis and exhibit negligible zero-order stray light in the projected images.

We can extend the technology to multiple spectral bands as illustrated in Fig. 2, where one BDOE produces either a

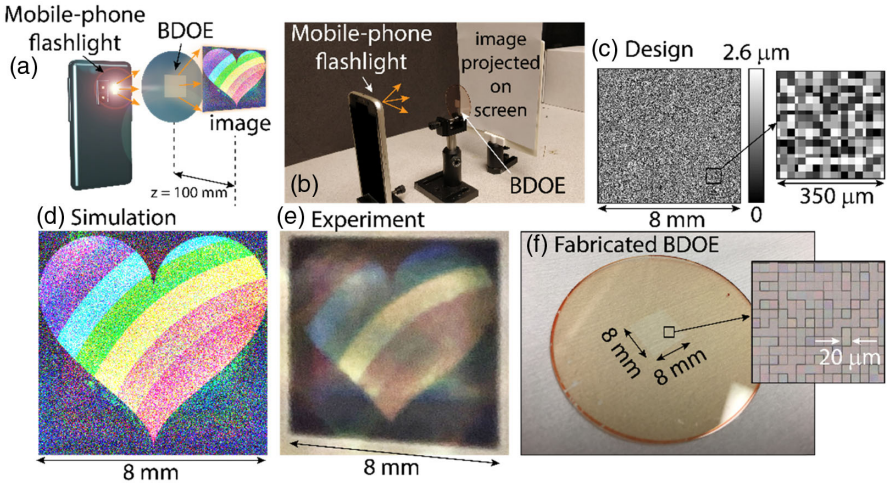

Fig. 1. BDOE illuminated by flashlight of a mobile phone. (a) Schematic and (b) photograph of the experimental setup. (c) Designed height map of the BDOE, showing (inset) magnified view of a small portion. (d) Simulated and (e) experimental full-color images when the BDOE is illuminated by the flashlight of a mobile phone. (f) Photograph showing a fabricated BDOE and (inset) optical micrograph of a small portion of the fabricated BDOE.

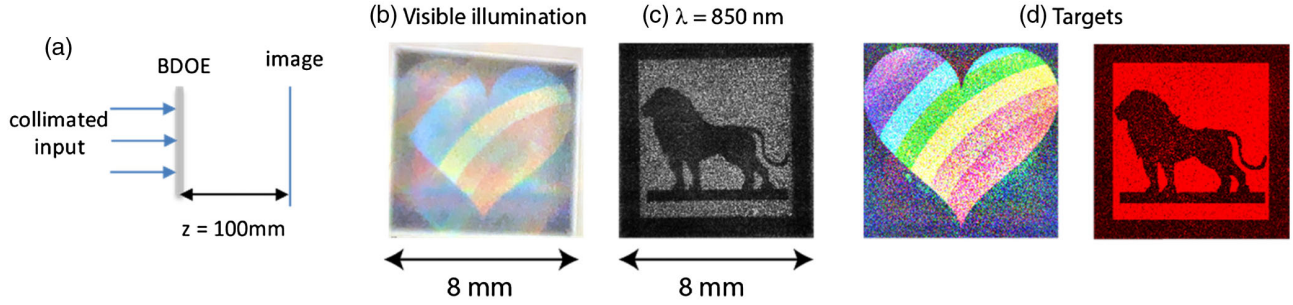

Fig. 2. Different images produced by one BDOE under different wavelengths. (a) Schematic of the experimental setup. Experimental images of (b) a rainbow heart with collimated light at λ = 400−700 nm (supercontinuum laser source) and (c) a lion silhouette with collimated light at 850 nm (bandwith = 15 nm). Target images are shown in (d). Also, see Visualization 1 for observations under sunlight.

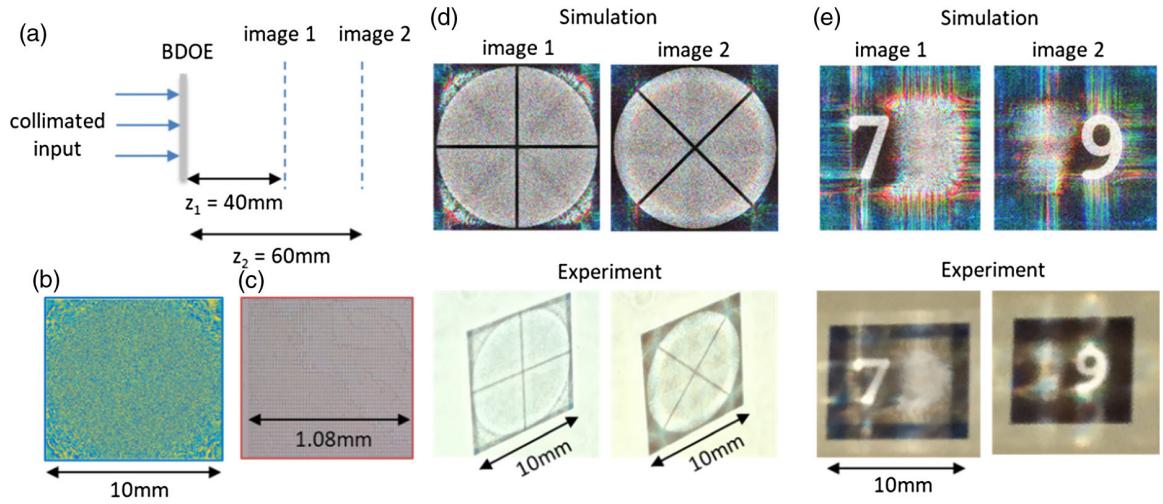

Fig. 3. Two different images produced by one BDOE at two different image planes. (a) Schematic of the experimental setup. (b) Designed height map of the BDOE. (c) Optical micrograph of a small portion of the fabricated BDOE. Simulated (top row) and experimental (bottom row) images of image 1 and image 2 for the BDOE in (c) are shown in (d) (Visualization 2 and Visualization 5), and for a different BDOE are shown in (e). The illumination was a collimated beam from a supercontinuum source ($\lambda = 400$ to 700 nm) and the cellphone flashlight was placed about 300 mm away from the BDOE for the "+/×" and the "7/9" devices, respectively. The experimental images were obtained by photographing the image projected onto a white screen.

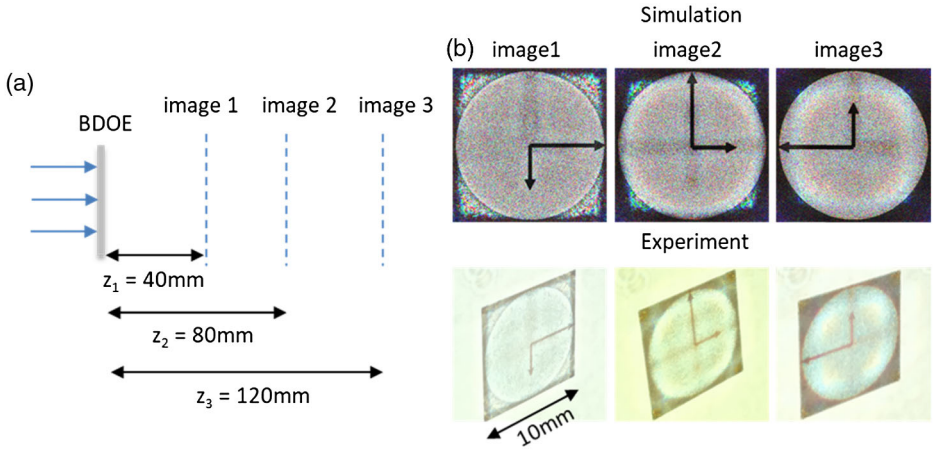

Fig. 4. Three different images produced by one BDOE at three different image planes. (a) Schematic of the experimental setup. (b) Simulated (top row) and experimental (bottom row) images of image planes 1, 2, and 3. The illumination was a collimated beam from a supercontinuum source ($\lambda = 400$ to 700 nm). The experimental images were obtained by photographing the image projected onto a white screen (Visualization 3 and Visualization 6).

full-color image or an invisible (near-IR) image when illuminated by a broadband white light [supercontinuum source with bandwidth of 400–700 nm, shown in Fig. 2(b)] or a near-infrared source [850 nm bandwidth = 15 nm, shown in Fig. 2(c)], respectively. We should mention that this is the same BDOE presented in Fig. 1. It is noteworthy that there is very little crosstalk between the two spectral bands. We analyzed the crosstalk by computing the structural similarity index maps (SSIMs) for the two planes and the global SSIM values, which for this case were 0.027 and 0.085 in the simulation and experiment, respectively. The average imaging efficiency was measured to be 54%, which is in close agreement with the simulated efficiency of 64%. Further details are presented in Ref. [7]. This was predicted via simulations before [5], but this is the first experimental demonstration to our knowledge. As a result, a single device enables both covert and overt security for anti-counterfeiting. In fact, under direct sunlight one can readily observe the rainbow heart, and by simply placing a visible-cut filter one can also observe the IR image of the lion (see Visualization 1).

In the Fresnel-diffraction regime, wavelength and propagation distance are interchangeable. Therefore, one would expect the BDOE to be able to project different images in different image planes as illustrated in Fig. 3 under monochromatic illumination [9]. In fact, we previously demonstrated this interchangeability in experiments with laser illumination [10]. However, this interchangeability is not obvious for broadband illumination. Here we show that even under broadband illumination, by appropriately designing the BDOE geometry, it is possible to control how the light intensity changes

upon free-space propagation. During the design phase, we maximized the imaging efficiency averaged over the multiple (discrete) planes and the multiple spectral bands simultaneously. When illuminated by collimated supercontinuum white light (SuperK EXTREME source and SuperK VARIA filter with $\lambda = 400-700$ nm), the BDOE shown in Figs. 3(b) and 3(c) projects image 1 ("+") at a distance of 40 mm and image 2 ("×") at a distance of 60 mm (see Visualization 2 and Visualization 5, showing the transition). Another pair of achromatic images (digits "7" and "9") projected by a different BDOE are shown in Fig. 3(e). In this case, the illumination was the white-LED flashlight of a mobile phone placed about 300 mm away from the BDOE, rendering the incident light collimated. Some crosstalk between the images in the different planes is observed. The global SSIM (crosstalk) in Fig. 3(d) between the two planes was 0.167 and 0.55 in the simulation and experiment, respectively [7]. In order to reduce the crosstalk, we can reduce the pixel width and increase the pixel height, as that will increase the imaging efficiency. We believe that this can be further mitigated by spacing the multiple planes farther apart.

The approach can be extended to three or more planes as well. In Fig. 4, we illustrate the example of three different images in three different planes (see Visualization 3 and Visualization 6). The illumination was collimated supercontinuum white light (SuperK EXTREME source and SuperK VARIA filter with $\lambda = 400 - 700$ nm). The global SSIM (crosstalk) in Fig. 4(b) between the first two planes was 0.133 and 0.74 in the simulation and experiment, respectively, that between the last two planes was 0.197 and 0.56 in the simulation and experiment, respectively, and that between the first and last planes was 0.125 and 0.67 in the simulation and experiment, respectively [7].

3. BDOE AS A LENS

Previously, we have shown broadband diffractive lenses for imaging [11–16]. In analogy with that work, here we show that the BDOE is equivalent to a lens, whose PSF is structured in the form of the desired image. If such a lens is illuminated by a collimated source (plane waves), it will form its PSF at a location equivalent to the focal plane. In the case of the BDOE, the desired image is produced at this plane. Elsewhere, the image would be blurred or out of focus. Extending this equivalence, when illuminated by a point source (spherical wave), it is expected of such a BDOE to project an image at a distance farther than the focal plane determined approximately by the well-known lens-maker's equation: $1/z_i + 1/z_s = 1/z_o$, where z_i, z_s, and z_o are the image distance, source distance, and "focal" distance, respectively, all measured from the BDOE [Fig. 5(a)]. In addition, the image formed is a convolution of the magnified PSF and the point source forming the incident spherical wave, where the magnification is determined approximately by z_i/z_s. The "focal" distance corresponds to the image distance used during design of the BDOE under collimated illumination. In Fig. 5(b), we experimentally show the measured values of z_s for various values of z_i for a BDOE with designed $z_0 = 38$ mm and the projected image of a white digit "5". The source is comprised of a white-LED light with an aperture in front in order to create an approximate point source. Collimation was achieved by placing this source at $z_s = 9$ m, where $z_i \sim z_0 = 38$ mm. The images formed by the same BDOE under supercontinuum collimated light (SuperK EXTREME and VARIA) and with magnification are shown in Figs. 5(c) and 5(d), respectively. Therefore, the BDOE is able to project images with magnification without the need for any additional optics. For the images in Fig. 5, we used a 300 μm pinhole in front of the LED flashlight to simulate spherical wave illumination. For illumination with supercontinuum collimated light, the full white spectrum (400–700 nm) was used. The illustrations, photographs, and further details of the imaging setups are provided in Ref. [7].

4. PLANAR AND REFLECTIVE BDOEs

BDOEs offer two other advantages. First, one can hide the geometry of the BDOE by utilizing a top coating as illustrated in Fig. 6(a), creating a flat BDOE. As long as the relative difference in refractive index (n_1 vs n_2) is non-zero, such devices can be designed in the same manner as conventional BDOEs. We show an example design of a flat BDOE in Fig. 6(b), where the top coating was polyvinyl alcohol (the patterned region was Shipley 1813 photoresist as in all the previous devices; see Ref. [7] for additional details). A layer of diluted polyvinyl alcohol (Sigma Aldrich, 0.001% by weight in water) was spin coated at 2000 rpm for 60 s on top of the fabricated BDOE. The simulated and experimental images under collimated white light are shown in Figs. 6(c) and 6(d), respectively (image distance = 50 mm). The image contrast is somewhat lower, but

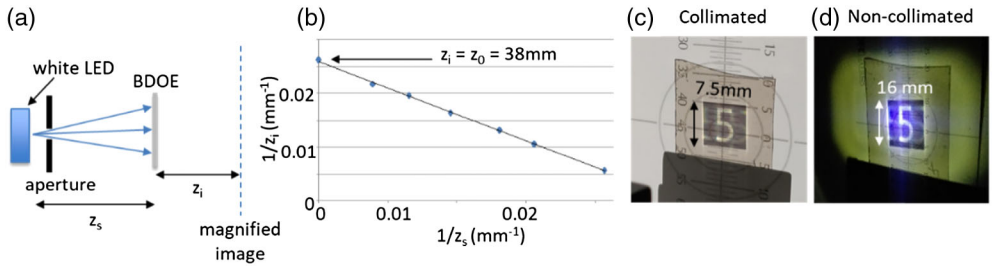

Fig. 5. Lensless image magnification with a BDOE. (a) Schematic of experimental setup. (b) The image formed by the BDOE satisfies the well-known lens-maker's equation, illustrating its equivalence to a lens. The image distance under collimated light z_0 is equivalent to the focal length of the lens. Images produced by this BDOE when illuminated by (c) collimated white light and (d) by non-collimated illumination showing magnification of the image (note the change in scale). The source was comprised of an opaque screen with a 0.3 mm diameter aperture placed in front of a white-LED flashlight (see Visualization 4 and Visualization 7). The distances (z_s and z_i) were about (9 mm and 40 mm) and (55 mm and 120 mm) in Figs. 5(c) and (d), respectively.

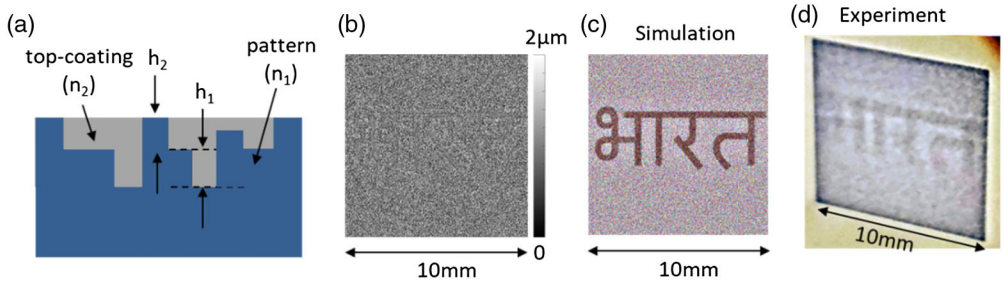

Fig. 6. Flat BDOE. (a) Schematic of a top coating on patterned layer to create a flat BDOE. (b) Design of a flat BDOE with pixel width of 20 μm and maximum pixel depth of 2.6 μm. Polyvinyl alcohol was used as the top-coating material. Image of this flat BDOE under white collimated light in (c) simulation and (d) via experiment.

this can be improved by using materials with higher refractive-index contrast or by increasing the maximum pixel depth. It is important to note that since meta-holograms have much higher aspect ratios than BDOEs, applying a top coating to render them flat is very challenging. Second, the minimum feature widths required for BDOEs are limited by diffraction, while meta-holograms require deep subwavelength constituent features and concomitantly high aspect ratios that are far more challenging to manufacture.

In some applications (for example, in packaging), one would require the BDOE to form an image in reflection as shown in the schematic in Fig. 7(a). We designed such a reflective BDOE by first depositing a reflective film (100 nm of Ag was deposited on a pristine glass wafer via sputtering with a 5 nm Cr layer in between for better adhesion using the Denton Discovery 18 sputter tool). The parameters of the sputtering process are given in Table S2 [7]. Further details of the sample inspection and related metrology are given in Section 3 of Ref. [7]. Then the photoresist was patterned using grayscale lithography as before [Fig. 7(b)]. The calibration procedure has to be carefully performed to account for the light reflections at the interfaces. Since the light undergoes two passes through the patterned

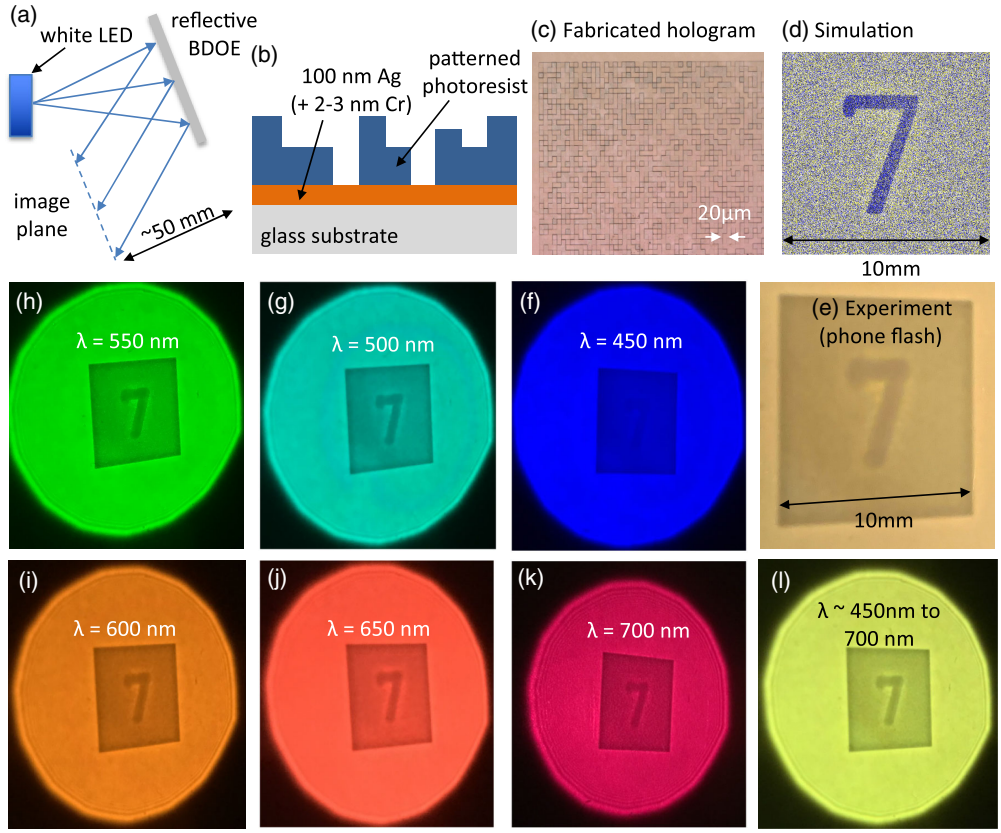

Fig. 7. Reflective BDOE. (a) Schematic showing the BDOE forming an image in reflection. (b) Schematic of the reflective BDOE microstructure. (c) Magnified optical micrograph of a portion of the fabricated reflective BDOE showing good pixel fidelity. (d) Simulated and (e)–(l) experimental image formed when illuminated by (e) a mobile-phone flashlight and (f)–(l) collimated laser light at normal incidence (close to normal incidence for the experiment) for different wavelengths (bandwidth = 50 nm). The illumination sources were (e) a white-LED flashlight from a mobile phone placed about 300 mm away from the BDOE and (f)–(l) collimated tunable supercontinuum source.

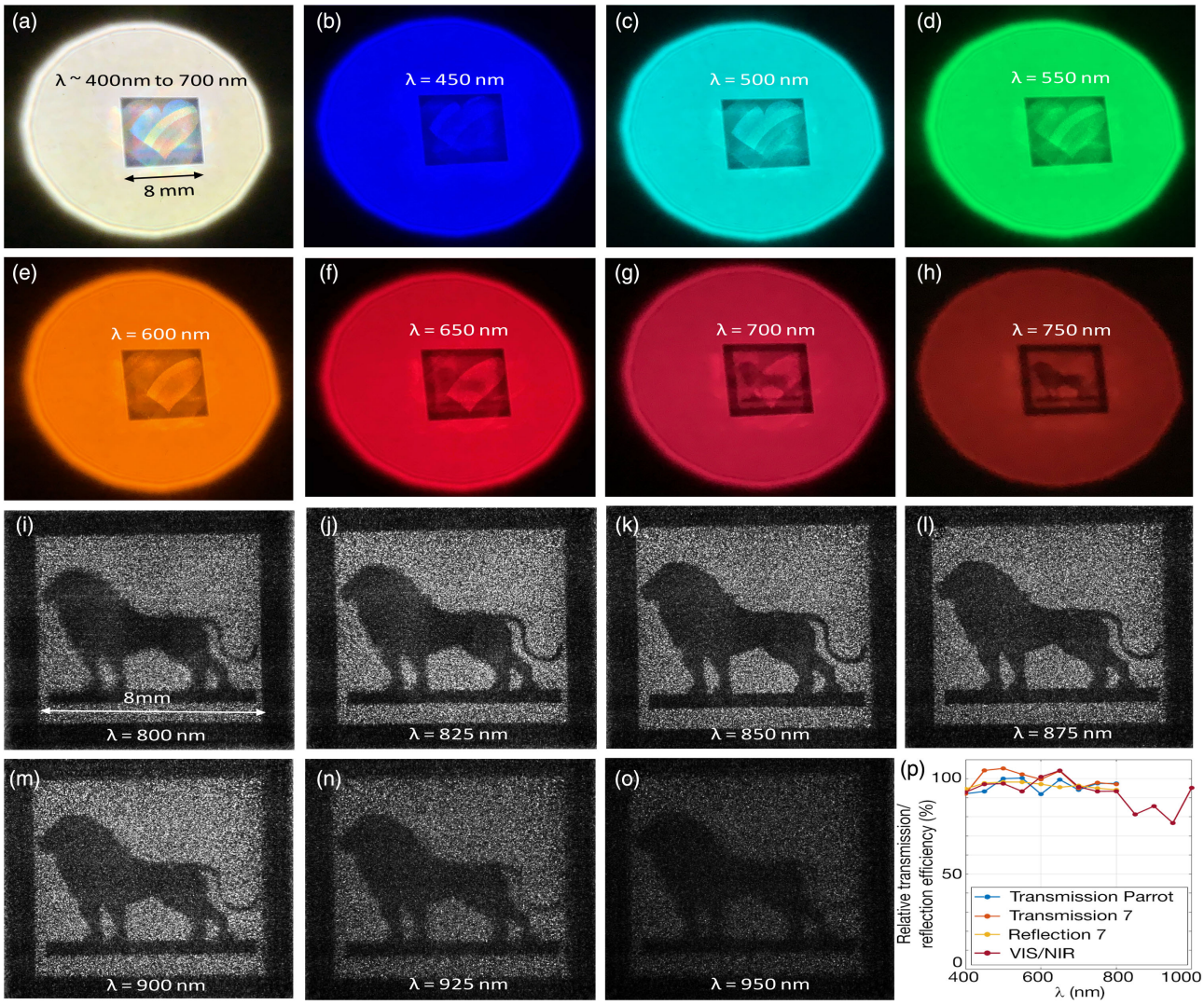

Fig. 8. Color-multiplexed images in a transmission rainbow heart (visible) and lion-silhouette (NIR) BDOE and transmission/reflection efficiency measurements. (a)–(o) Images produced by the BDOE when illuminated by collimated tunable supercontinuum source with (a) broadband (400–700 nm) and (b)–(o) narrowband (bandwidth = 50 nm) illumination. The images (i)–(o) were captured by projecting the image on a CMOS sensor, since the camera used to capture images (a)–(h) was not capable of photographing in the IR band. In (a), minimal tone adjustment was performed to remove an extraneous yellow tint from the image that was present in the photograph but not seen with the naked eye. No other image processing has been performed. (p) Relative transmission/reflection efficiency spectra of the BDOE (VIS/NIR) shown in (a)–(o), reflective BDOE shown in Fig. 7 (Reflection 7), and other transmissive BDOE (transmission parrot and 7, not shown here) that project images of a parrot and a "7" in transmission. Details of the measurements are in Ref. [7].

photoresist, the associated phase shift is doubled (at normal incidence). An optical micrograph of a portion of the fabricated device is shown in Fig. 7(c) with pixel width = 20 μm. The image formed at a distance of 50 mm when illuminated by a mobile-phone flashlight and collimated white laser light is shown via simulation and via experiment in Figs. 7(d)–7(f), respectively. The experiment was performed at a small incidence angle as illustrated in Fig. 7(a). It is possible to obtain full-color images in this scenario if one takes into account the reflection spectrum of the reflective film used. In our preliminary demonstration, we did not account for this effect. Nevertheless, we showed good achromatic image projection by capturing the images at narrowband and broadband illumination using a tunable supercontinuum source [see Figs. 7(f)–7(i) and Ref. [7]). As far as we are aware, this is the first demonstration of a reflective image-projecting hologram that is achromatic over the visible band (450–700 nm).

In Fig. 8, we showcase the color multiplexing capability of a transmission BDOE that projects the image of a rainbow heart (when illuminated with visible light) and lion silhouette (when illuminated with NIR light). It can be seen that the same device projects the rainbow heart pattern in the visible band and the lion silhouette in the NIR band. It is interesting to note that the lion silhouette starts appearing at around 700 nm illumination and becomes dominant until 900 nm (images up to 950 nm illumination are shown in Ref. [7]).

Excellent color fidelity is observed under both the (a) broadband and (b-o) narrowband illumination. We also measured

the transmission efficiency of four different BDOEs, and the results are summarized in Fig. 8(p). The relative transmission/reflection efficiency is measured as the ratio of power transmitted/reflected by the BDOE to the power transmitted/reflected by a reference (unpatterned) device. As was pointed out previously [4], the multi-level microstructures function as an anti-reflection coating, which enables the relative efficiency to go above 100% at certain wavelengths. The average transmission efficiencies from 400 to 800 nm are over 96% for all four measured BDOEs and ∼85% for the VIS/NIR BDOE in the 850–1000 nm range. Details of these measurements are included in Ref. [7]. We emphasize that transmission efficiency is somewhat unrelated to the imaging efficiency. The latter measures the fidelity of the projected images, while the former simply states how much power is transmitted.

5. CONCLUSIONS

In summary, here we demonstrate that appropriate design of multi-level diffractive structures can enable efficient image projection over broadband and multiple spectral bands as well as onto multiple image planes. Since such structures may be fabricated at low cost over large areas and at high speed via various imprinting technologies, [17] these can be readily used in anti-counterfeiting applications. We note that nano- and micro-optical elements are already prevalent in huge volumes in many consumer electronics and banknotes [18]. In addition, we point out that metamaterials and metasurfaces for image projection do not offer any advantage over BDOEs. In fact, BDOEs are far easier to manufacture due to (1) their much larger feature widths, (2) their much smaller aspect ratios, and (3) their use of low-index polymers that are readily amenable to imprinting. Their differences have been discussed in some detail in Ref. [11] in the context of imaging. Since spatial frequencies that are larger than $2\pi/\lambda$ do not propagate in free space, there is no need for pixel widths smaller than $\lambda/2$. This also means that even though meta-holograms have pixels with widths far smaller than the wavelength, the free-space propagation cutoff limits information transfer to the same spatial frequencies as in the case of BDOEs. In other words, meta-holograms cannot transmit any additional information than BDOEs into the regions of space farther than a few wavelengths away. We do note that meta-holograms have unique advantages over BDOEs in the case of polarization- or spin-encoded holography [19–22]. But these suffer from poor efficiency and require sub-100 nm structures, which are challenging to manufacture over large areas.

Funding. Office of Naval Research (N66001-10-1-4065); Utah Science Technology and Research (USTAR).

Acknowledgment. We thank Brian Baker, Steve Pritchett, and Christian Bach for fabrication advice and Christian Skipper (Keyence) for providing the 3D optical micrograph.

Disclosures. RM: Oblate Optics, Inc. (I); University of Utah (P).

†These authors contributed equally to this work.

REFERENCES

1. J. Cho, S. Kim, S. Park, B. Lee, and H. Kim, "DC-free on-axis holographic display using a phase-only spatial light modulator," Opt. Lett. **43**, 3397–3400 (2018).
2. M. Khorasaninejad, A. Ambrosio, P. Kanhaiya, and F. Capasso, "Broadband and chiral binary dielectric meta-holograms (supplementary materials)," Sci. Adv. **2**, e1501258 (2016).
3. L. Wang, S. Kruk, H. Tang, T. Li, I. Kravchenko, D. N. Neshev, and Y. S. Kivshar, "Grayscale transparent metasurface holograms," Optica **3**, 1504–1505 (2016).
4. N. Mohammad, M. Meem, X. Wan, and R. Menon, "Full-color, large area, transmissive holograms enabled by multi-level diffractive optics," Sci. Rep. **7**, 5789 (2017).
5. G. Kim, J. A. Domínguez-Caballero, and R. Menon, "Design and analysis of multi-wavelength diffractive optics," Opt. Express **20**, 2814–2823 (2012).
6. K. T. P. Lim, H. Liu, Y. Liu, and J. K. W. Yang, "Holographic colour prints for enhanced optical security by combined phase and amplitude control," Nat. Commun. **10**, 25 (2019).
7. M. Meem, A. Majumder, and R. Menon, "Multi-plane, multi-band image projection via broadband diffractive optics," arXiv:1901.05943 (2019), Supplementary Information.
8. Y. Deng and D. Chu, "Coherence properties of different light sources and their effect on the image sharpness and speckle of holographic displays," Sci. Rep. **7**, 5893 (2017).
9. J. W. Goodman, *Introduction to Fourier Optics*, McGraw-Hill Series in Electrical and Computer Engineering (1996).
10. P. Wang and R. Menon, "Optical microlithography on oblique and multiplane surfaces using diffractive phase masks," J. Micro/Nanolithogr. MEMS MOEMS **14**, 023507 (2015).
11. S. Banerji, M. Meem, A. Majumder, F. G. Vasquez, B. Sensale-Rodriguez, and R. Menon, "Imaging with flat optics: metalenses or diffractive lenses?" Optica **6**, 805–810 (2019).
12. M. Meem, S. Banerji, A. Majumder, F. G. Vasquez, B. Sensale-Rodriguez, and R. Menon, "Broadband lightweight flat lenses for longwave-infrared imaging," Proc. Natl. Acad. Sci. USA **116**, 21375–21378 (2019).
13. M. Meem, A. Majumder, and R. Menon, "Full-color video and still imaging using two flat lenses," Opt. Express **26**, 26866–26871 (2018).
14. N. Mohammad, M. Meem, B. Shen, P. Wang, and R. Menon, "Broadband imaging with one planar diffractive lens," Sci. Rep. **8**, 2799 (2018).
15. M. Meem, S. Banerji, A. Majumder, C. Dvonch, B. Sensale-Rodriguez, and R. Menon, "Imaging across the short-wave infra-red (SWIR) band via a flat multilevel diffractive lens," OSA Continuum **2**, 2968–2974 (2019).
16. S. Banerji, M. Meem, A. Majumder, and B. Sensale-Rodriguez, "Imaging over an unlimited bandwidth with a single diffractive surface," arXiv:1907.06251v1 (2019).
17. I. Moreno, A. Martinez-Garcia, L. Nieradko, J. Albero, and C. Gorecki, "Low-cost production of computer-generated holograms: from design to optical evaluation," J. Eur. Opt. Soc. **5**, 10011 (2010).
18. N. P. Mahalik, *Micromanufacturing and Nanotechnology* (Springer, 2006).
19. F. Cheng, L. Ding, L. Qiu, D. Nikolov, A. Bauer, J. P. Rolland, and A. N. Vamivakas, "Polarization-switchable holograms based on efficient, broadband multifunctional metasurfaces in the visible regime," Opt. Express **26**, 30678–30688 (2018).
20. R. Zhao, B. Sain, Q. Wei, C. Tang, X. Li, T. Weiss, L. Huang, Y. Wang, and T. Zentgraf, "Multichannel vectorial holographic display and encryption," Light Sci. Appl. **7**, 95 (2018).
21. Q. Wang, E. Plum, Q. Yang, X. Zhang, Q. Xu, Y. Xu, J. Han, and W. Zhang, "Reflective chiral meta-holography: multiplexing holograms for circularly polarized waves," Light Sci. Appl. **7**, 25 (2018).
22. J. Kobashi, H. Yoshida, and M. Ozaki, "Circularly-polarized, semi-transparent and double-sided holograms based on helical photonic structures," Sci. Rep. **7**, 16470 (2017).